THE JOURNAL OF PHYSICAL CHEMISTRY B

Article

pubs.acs.org/JPCB

Analysis of Biomolecular Solvation Sites by 3D-RISM Theory

Daniel J. Sindhikara[†] and Fumio Hirata*[,‡]

[†]Department of Science and Engineering, and [‡]College of Life Sciences, Ritsumeikan University, Kusatsu, Shiga 525-8577, Japan

ABSTRACT: We derive, implement, and apply equilibrium solvation site analysis for biomolecules. Our method utilizes 3D-RISM calculations to quickly obtain equilibrium solvent distributions without either necessity of simulation or limits of solvent sampling. Our analysis of these distributions extracts highest likelihood poses of solvent as well as localized entropies, enthalpies, and solvation free energies. We demonstrate our method on a structure of HIV-1 protease where excellent structural and thermodynamic data are available for comparison. Our results, obtained within minutes, show systematic agreement with available experimental data. Further, our results are in good agreement with established simulation-based solvent analysis methods. This method can be used not only for visual analysis of active site solvation but also for virtual screening methods and experimental refinement.

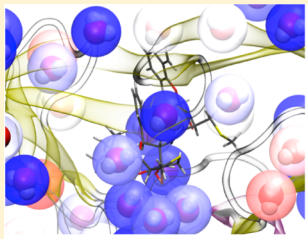

Solvation site poses and energies from 3D-RISM

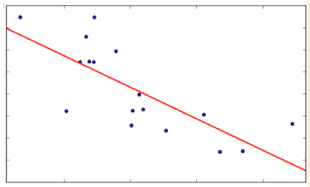

RMSD error with experiment correlated with $-T\Delta S$[1]

1. INTRODUCTION

Solvent plays several critical roles in the function of biomolecules. In particular, microscopic effects of solvent such as hydrogen bonding and binding affinity augmentation by the "solvent-displacement effect" are necessary for critical analysis of ligand binding. Minute knowledge of such effects is necessary for reliable prediction, explanation, and design of molecular systems. Thus, it is no wonder increasing attention is paid by the pharmaceutical-design community to solvent molecules inside the active site of proteins.

Experimental methodologies for analyzing atomistic water behavior can be extremely useful but are often hindered by limited spatial resolution. Sophisticated theoretical analysis of water based on simulation has been in development for over a decade. In 1998, Lazaridis derived inhomogeneous fluid solvation theory (IFST) in two landmark papers.[1,2] Several years later, Young et al. developed a solvation site-based approach, commonly called "Watermap", to the forefront by applying IFST toward identification of displaceable water sites to enhance ligand binding.[3,4] Similarly, recent work by Nguyen et al. uses, rather, a grid-based application of IFST called "GIST".[5] Although the "explicit-solvent" simulations, on which this analysis is based, enable incredible precision, the sampling problem limits reliable analysis to smaller systems depending on the available computational budget. Even for extremely expensive simulations, however, it is questionable whether sufficient sampling of water and ions has occurred in buried regions of the solute where the solvent exchange rate is very slow.[6−9]

Here, we circumvent the solvent sampling problem by using the three-dimensional reference interaction site model (3D-RISM) theory.[10,11] 3D-RISM attains complete atomistic sampling of solvent, including ions, by utilizing an integral approach. 3D-RISM has been successful in locating water in proteins as compared to experiment[12−15] and simulation,[16,17] ion locations and pathways,[18−20] hydration free energies,[21] fragment poses,[14,22−24] and drug poses,[24,25] as well as many more applications less relevant to this work. With current implementations, the equilibrium solvent distribution of a biologically relevant system can be calculated in minutes to hours. Further implementation improvements such as numerical optimizations[26] and GPU implementations[27] continue to further reduce the 3D-RISM calculation time. While most analysis of 3D-RISM water hydration sites has been qualitative, recent work has allowed for automatic prediction of water and ion site locations with excellent agreement against high-resolution experimental data.[15,28]

Here, we create an analysis suite including adaptations of IFST as well as geometrical analysis toward 3D-RISM. We demonstrate the capabilities of this algorithm first qualitatively through observation of hydrogen bonding in alanine dipeptide, then quantitatively comparing against available experimental geometrical and thermodynamic data of solvation in HIV-1 protease.

2. THEORETICAL METHODS

2.1. 3D-RISM Theory. Since 3D-RISM has been established for years, here we only briefly summarize the principles.[10,11] 3D-RISM is a 3D, solvent "interaction-site"-based interepretation of the molecular Ornstein−Zernike equation. 3D-RISM first utilizes RISM calculations to find the susceptibility function of the solvent based on specified atomic interaction potentials and mixture concentrations. The solvent susceptibility is then utilized in the 3D-RISM equations, including the atomic

Received: May 9, 2013
Revised: May 14, 2013
Published: May 15, 2013

   dx.doi.org/10.1021/jp4046116 | J. Phys. Chem. B 2013, 117, 6718−6723

solvent−solute interaction potential. The 3D-RISM equations coupled with an appropriate closure relation are iterated until self-consistency resulting in the 3D solvent distribution function $g(\mathbf{r})$, the total correlation function $h(\mathbf{r})$, the direct correlation $c(\mathbf{r})$, as well as other distributions and properties. Thus, equilibrium solvation properties are obtained without necessity for a dynamic simulation.

2.2. Computational Algorithm. *2.2.1. General Protocol.* Our method begins by running a standard 3D-RISM calculation on a static solute structure. The rest of the analysis, as described below, is postprocessing of standard 3D-RISM output distributions including $g(\mathbf{r})$, $h(\mathbf{r})$, $c(\mathbf{r})$, and $u(\mathbf{r})$ (the local interaction potential). Each solvation site is located and then characterized (geometrically and thermodynamically) sequentially until a cutoff is reached (as described below). Although no simulation is required, because the calculation is completely dependent on the solute structure, some cases may call for an initial molecular dynamics simulation or minimization to optimize the solute structure/structural ensemble.

2.2.2. Determining Site Locations. To characterize solvation sites, we must first identify its location. We have previously published an algorithm, *Placevent*, that has successfully identified water and ion sites using a particle conservation law applied to 3D-RISM data according to the following equations:

$$P(\mathbf{r})_0 = \rho_0 g(\mathbf{r})_0 \tag{1}$$

$$\int_{r_n^{\max}}^{R_n} P(\mathbf{r})_n \, d\mathbf{r} = 1 \tag{2}$$

$$P(\mathbf{r})_n = P(\mathbf{r})_{n-1} \times (1 - \Theta(|\mathbf{r} - \mathbf{r}_{n-1}^{\max}| - R_{n-1})) \tag{3}$$

where $P(\mathbf{r})$ is the local population function, $r^{\max}$ is the location with maximum probability, and R_n is the nth radius to satisfy eq 2. In *Placevent*, discrete atoms are added at $\mathbf{r}_n^{\max}$, iteratively according to eq 3, until $P(\mathbf{r}^{\max})$ drops below some preset cutoff indicating that "enough" solvent molecules have been placed. This particle conservation algorithm is useful for identifying a realistic snapshot of solvent locations. Here, because we are interested in identifying all solvation sites, we prefer a more promiscuous algorithm, allowing even partially occupied sites (i.e., not enforcing one site per particle). Thus, we fix R_n to be some preset (small) radius R. Here, we still use eq 1, eq 2 is unnecessary, and we replace eq 3 with:

$$P(\mathbf{r})_n = P(\mathbf{r})_{n-1} \times (1 - \Theta(|\mathbf{r} - \mathbf{r}_{n-1}^{\max}| - R)) \tag{4}$$

Similar to *Placevent*, this algorithm is iterated until a cutoff is reached; here, we cut off at a number of solvent molecules placed. The resulting discrete distribution represents high occupancy "solvation sites", which will be subject to further analysis (see below).

2.2.3. Determining Orientational Distribution. Imai et al. introduced an algorithm for the identification of the most likely orientation of a solvent molecule using 3D-RISM distribution data in the context of fragment mapping.[22] That method scores the unnormalized probability of a certain pose of a solvent molecule by superimposing the distributions of each solvent site in the corresponding pose location. Here, we will use a similar method with some optimizations.

In Imai's work, rotational space is searched using incrementation of Euler rotation angles (a technique that is called "variable stepping").[29] This technique, while straightforward to implement, has recently been shown to be nonoptimal with respect to coverage of orientational space in a work by Mitchell.[30] Our own testing (data not shown) supports that the variable stepping technique results in gaps in coverage, leading to inefficient orientational sampling. Thus, we employed rather the Successive Orthogonal Images (SOI) approach, which has been shown to produce more uniform coverage.[30,31] Here, we briefly describe the SOI approach:

(1) Create a uniform distribution of points on the unit sphere, V^1.
(2) For each point on the sphere, create a set of uniform vectors, V^2, also within the unit sphere, which are orthogonal to the vector pointing from the center to that point.
(3) Determine an orthogonal vector to the two previous vectors.
(4) Determine the rotation, M, expressed in Euler angles corresponding to the three orthogonal vectors based on an arbitrary reference geometry.

The resulting set of rotations exists within $SO(3)$ and represents a uniform set of rotations. For efficiency in computation, we find the optimal angular difference, α, and sizes of $|V^1|$ and $|V^2|$ for a fixed number of rotations, N_{rot}. Equation 3.1 in Mitchell's work[30] shows that $|V^2| = 4\pi/\alpha^2$ and $|V^1| = 2\pi/\alpha$; thus we set $\alpha = (8\pi^2/N_{\text{rot}})^{1/3}$, where $N_{\text{rot}} = |V^2|\cdot|V^1|$.

For our purposes, we assign the solvent atom closest to the center of mass (oxygen for water) as a fixed, "anchor" for rotations. For each position of an anchor, the rotational probability distribution function can be described as:

$$P(\omega|\mathbf{r}_{\text{anchor}}) = Z^{-1} \prod_{\gamma \in \text{sites}} g_\gamma(\mathbf{r}_{\text{anchor}} + \mathbf{r}_{\gamma,\omega}) \tag{5}$$

Here, $\mathbf{r}_{\gamma,\omega}$ is the relative position of the solvent-site γ given rotation ω from some arbitrary original geometry, and Z is the partition function. $g_\gamma(\mathbf{r}_{\text{anchor}} + \mathbf{r}_{\gamma,\omega})$ is calculated using a linear interpolation of the eight nearest grid points. The solvation site is defined as the 6D conformational space available by moving the anchor atom within a 1.0 Å radius sphere centered on the originally identified location, $\mathbf{r}_n$. The highest likelihood pose lies at the maximum of $P(\omega|\mathbf{r})$ where $|\mathbf{r} - \mathbf{r}_n| \leq R$.

2.2.4. Solvation Site Characterization. We characterize "solvation sites" using integrations over the solvation site volume. The excess chemical potential or solvation free energy can be evaluated simply using the total and direct correlation functions for a variety of 3D-RISM closures including the KH-closure, which we use here.[11,32]

$$\Delta\mu_n^{\text{KH}} = \rho_0 k_B T \sum_\gamma \int_{V_n} \left[\frac{1}{2}(h_\gamma(\mathbf{r}))^2 \Theta(-h_\gamma(\mathbf{r}) - c_\gamma(\mathbf{r})) - \frac{1}{2} h_\gamma(\mathbf{r}) c_\gamma(\mathbf{r}) \right] d\mathbf{r} \tag{6}$$

Here, V_n is the volume of the nth solvation site. For the partial molar volume, we straightforwardly use the adapted Kirkwood−Buff equations toward 3D-RISM data:[33]

$$\bar{V}_n = k_B T \chi_T^0 \left(1 - \rho_0 \sum_\gamma \int_{V_n} c_\gamma(\mathbf{r}) \, d\mathbf{r} \right) \tag{7}$$

For the energy and entropy, for practical purposes, we use only the terms first order in the density, that is, the excess solute−solvent terms. The general forms are adapted from the GIST expressions[5] rooted in Lazaridis' work.[1,2]

dx.doi.org/10.1021/jp4046116 | J. Phys. Chem. B 2013, 117, 6718−6723

$$E_n^1 = \rho_0 \sum_\gamma \int_{V_n} g_\gamma(\mathbf{r}) u_\gamma(\mathbf{r})\, d\mathbf{r} \tag{8}$$

$$S_n^{1,\mathrm{trans}} = -\rho_0 k_B \int_{V_n} g_{\mathrm{anchor}}(\mathbf{r}) \ln g_{\mathrm{anchor}}(\mathbf{r})\, d\mathbf{r} \tag{9}$$

For the orientational entropy, we need an expression for $g(\omega|\mathbf{r})$ (which is not readily available from 3D-RISM output). We use the expression from eq 5 for the probability written in terms of g: $g(\omega|\mathbf{r}) = N_{\mathrm{rot}}\rho(\omega|\mathbf{r})$, where N_{rot} is the total number of rotations.

Using the above equations, we can straightforwardly write the expression:

$$S_n^{1,\mathrm{trans}} = -\frac{\rho_0 k_B}{N_{\mathrm{rot}}} \int_{V_n} g_{\mathrm{anchor}}(\mathbf{r})\, d\mathbf{r} \int_\omega g(\omega|\mathbf{r}) \ln g(\omega|\mathbf{r})\, d\omega \tag{10}$$

The normalization factor $1/N_{\mathrm{rot}}$ is different from the usual $1/8\pi^2$ in accordance with the rotational entropy normalization condition in eq 5 of ref 34.

3. RESULTS AND DISCUSSION

3.1. Calculation Parameters. Two systems, alanine dipeptide and an inhibitor-bound form of HIV-1 protease, were examined. The alanine dipeptide structure and all parameters were prepared using tLEaP.[35] For HIV-1 protease, a combined X-ray and neutron crystallography structure was used (PDB ID: 2ZYE).[36] Protein interaction parameters were taken from the ff99SB parameter set.[37] The bound HIV-1 protease inhibitor, KNI-272, was parametrized with Gaussian 09[38] using HF 6-31G* basis set and GAFF parameters[39] using antechamber[40] with RED IV[41] parametrization. Protonation states were taken from available deuterium data from the experimental structure. Pure water at 55.5 M used modified SPC parameters.[42] 3D-RISM calculations were run using the AmberTools rism3d.snglpnt.MPI module.[35,42] All calculations were performed on an HP Z100 8-core Intel 3.2 GHz Xeon workstation. The 3D-RISM calculation on HIV-1 protease and alanine dipeptide using the KH closure took 6.5 min and 39 s, respectively. Postprocessing was performed using a Python script, which took 4.3 min to run in serial.

3.2. Pose Visualization on Alanine Dipeptide. To get a visual perspective on the posed waters in the context of the 3D-RISM distributions, we first analyzed a digestibly small system, alanine dipeptide. As can be seen in Figure 1, the posed water molecules loosely obey the 3D-RISM distribution in a manner where they do not overcrowd each other. Further, apparent water hydrogen bonding occurs between a water oxygen and each NH hydrogen (1.79 and 2.39 Å) as well as between a water hydrogen and each C═O oxygen (1.70 and 2.24 Å). These results suggest that this method gives qualitatively reasonable positions and orientations.

3.3. Analysis of HIV-1 Protease. *3.3.1. Comparison to Experimental Data.* We compared our predicted water data to the combined neutron and X-ray crystallography structure of HIV-1 protease bound to an inhibitor (PDB ID: 2ZYE),[36] which contains many well-resolved water poses. Out of the 87 complete water molecules reported in the experimental data and our 100 predicted water molecules (the number 100 was chosen arbitrarily), there were only 32 cases where water oxygen atom positions coincided by less than 1.5 Å. The atomic-distance RMSD between these pairs ranged between 0.48 and 2.07 Å.

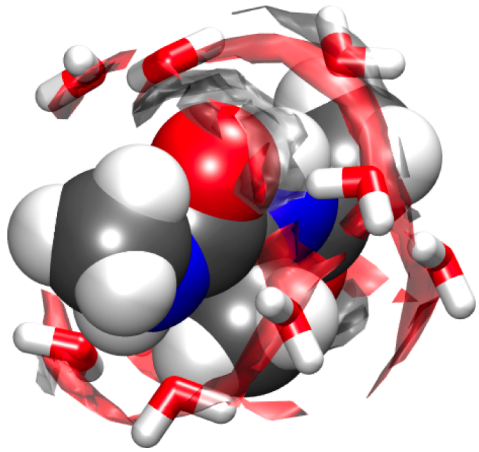

Figure 1. Posed waters and 3D-RISM distribution near alanine dipeptide. 3D-RISM isosurfaces are shown at $g(\mathbf{r}) = 2$ in translucent gray for hydrogen and at $g(\mathbf{r}) = 3$ in translucent red for oxygen.

For both prediction and experiment, however, some uncertainty in position is expected in places where the solvent molecule is not tightly bound. We expect that the diversity of available poses within each site should roughly be related to its entropy. In Figure 2a–d, we compared experimental water molecules to their nearest predicted solvation site and compared the atomic distance RMSD between the pair of poses (experimental and predicted) with $-T\Delta S^1$. Linear fits give Pearson's correlation coefficients of $r = -0.47$ and $r = -0.67$ for $-T\Delta S^{1,\mathrm{trans}}$ and $-T\Delta S^{1,\mathrm{rot}}$, respectively. The strongest correlation was with the total contribution of entropy to the free energy, $-T\Delta S^1$ where $r = -0.76$. $-T\Delta S^{1,\mathrm{trans}}$ had a $r = -0.48$ against distance between experimental and predicted oxygens. Although we do not necessarily argue that these relationships should be linear, our data suggest that there is a reasonable correlation between "structural predictability" and entropy. This systematic effect would be invisible if we had unsatisfactory experimental structures, predicted poses, or predicted entropy, suggesting that our predictions and the corresponding experimental orientations are reasonable.

We observed additional correlations such as the experimental B-factor also had a correlation of $r = 0.46$ with the O–O distance, and ΔE^1 with $-T\Delta S^1$ with an $r = -0.58$ (suggesting entropy–enthalpy compensation).

3.3.2. Comparison to Simulation. Next, we quantitatively compare our thermodynamic quantities to those obtained by simulation-based IFST analysis. In 2003, Li and Lazaridis[43] studied an isolated water bound between the flaps and the potent inhibitor, KNI-272-bound form of HIV-1 protease, using structure 1HPX[44] and the simulation-based approach. Although many published studies exist utilizing IFST, this simulation study is uniquely useful because we can unambiguously identify the water location (because this flap water is completely isolated).

In Table 1, we compare their data versus those from our 3D-RISM-based approach. For this water site, our estimates for solvation free energy agreed to less than 1 kcal/mol. We predicted less $-T\Delta S^1$ (more entropy) than their estimates by 1–2 kcal/mol. We also predicted less solvent–solute interaction energy (ΔE^1) by about 7 kcal/mol. We believe the large error in energy is caused mostly by a technical problem with the grid-based storage of energies (eq 8) and can be solved by modifying the 3D-RISM code itself (it is not

dx.doi.org/10.1021/jp4046116 | J. Phys. Chem. B 2013, 117, 6718–6723

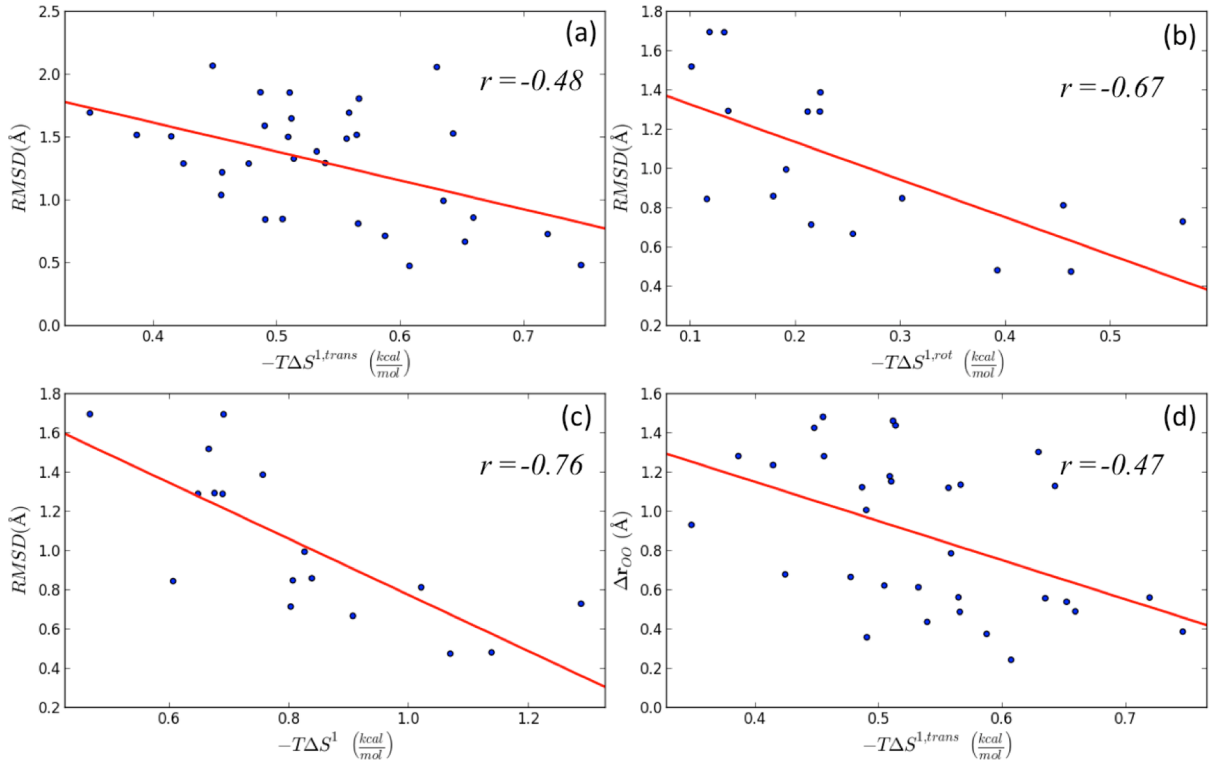

Figure 2. (a–d) Correlations between entropy and agreement with experiment. RMSD and distance comparisons are between predicted and nearest experimental water. Appropriately, the agreement with experiment is consistently better with lower entropy (higher $-T\Delta S^{1}$).

Table 1. Comparison of Thermodynamic Properties of Selected Water Sites in HIV-1 Protease[a]

location	flap			active site	termini	hinge
crystal water index	301	301	301	354	308	none
study	Li et al. 8 ns	Li et al. 1 ns	present study	present study	present study	present study
$\Delta\mu$ (kcal/mol)	−15.2	−15.9	−15.96	−4.96	+1.65	−0.93
$-T\Delta S^{1,rot}$ (kcal/mol)	1.47	n/a	0.39	0.30	0.09	0.05
$-T\Delta S^{1,trans}$ (kcal/mol)	1.47	n/a	0.75	0.50	0.12	0.18
$-T\Delta S^{1}$ (kcal/mol)	2.94	3.30	1.14	0.81	0.21	0.23
ΔE^{1} (kcal/mol)	−28.2	−28.0	−35.2	−12.21	−0.23	−5.87
$p\Delta V$ (kcal/mol)	∼0	∼0	0.01	0.00	0.00	0.01

[a]Comparison of 3D-RISM-based thermodynamic properties calculated here vs simulation-based properties calculated by Li and Lazaridis on the same "flap water" in HIV-1 protease.

possible to correct using postprocessing). Other sources of disagreement may be partly attributed to differences in force field and solute structures; other factors are likely due to limitation of methodological errors for generating the initial data (sampling error in simulation and closure error in 3D-RISM).

Note that Li and Lazaridis' work calculates the total solvation free energy by addition of explicit terms. The work here calculates only the first-order terms in energy and entropy but calculates the solvation free energy directly.

The site in the vicinity of KNI-272, the "flap" water, despite its steep entropic penalty, favorably contributes to the solvation free energy. Our analysis found even less favorable waters including, for example, nearby the inhibitor crystal water 354 ΔG = −4.96 kcal/mol, in a largely hydrophobic pocket near residues I15, I33, L38, M36, and V88 in the hinge region, ΔG = −0.93 kcal/mol, and near crystal water 308 near the termini with ΔG = +1.65 kcal/mol. These additional sites, as seen in Table 1, have significantly less favorable solute-interaction energies.

4. CONCLUSIONS

In summary, we have developed an algorithm for analyzing poses and thermodynamics of solvation sites without the need for simulations; thus we are circumventing the solvent sampling problem. Our method shows systematic agreement with high-resolution experimental data and with simulation-based water analysis techniques. Our calculations on HIV-1 protease took just under 11 min in total (3D-RISM + postprocessing) on an 8-core workstation. Further, this method can directly take into account cosolvent and ionic effects on solvent structure and thermodynamics via additional, fast 3D-RISM calculations. Thus, we assert that our method is both extremely practical and reasonably accurate method for solvation site analysis. Our future work will include a much larger, systematic analysis of this method for large number of systems including a more critical comparison to inhomogeneous fluid solvation theory simulation-based methods.

dx.doi.org/10.1021/jp4046116 | J. Phys. Chem. B 2013, 117, 6718–6723

AUTHOR INFORMATION

Corresponding Author

*E-mail: hirataf@fc.ritsumei.ac.jp.

Notes

The authors declare no competing financial interest.

ACKNOWLEDGMENTS

This work and D.J.S. were supported by the Grant-in Aid for Scientific Research from the MEXT in Japan. We would like to acknowledge David Case for discussion on the alanine dipeptide solvent structure and Ronald Levy for suggestion on the goals of this work.

REFERENCES

(1) Lazaridis, T. Inhomogeneous Fluid Approach to Solvation Thermodynamics. 1. Theory. *J. Phys. Chem. B* **1998**, *102*, 3531−3541.

(2) Lazaridis, T. Inhomogeneous Fluid Approach to Solvation Thermodynamics. 2. Applications to Simple Fluids. *J. Phys. Chem. B* **1998**, *102*, 3542−3550.

(3) Young, T. T.; Abel, R. R.; Kim, B. B.; Berne, B. J. B.; Friesner, R. A. R. Motifs for Molecular Recognition Exploiting Hydrophobic Enclosure in Protein-Ligand Binding. *Proc. Natl. Acad. Sci. U.S.A.* **2007**, *104*, 808−813.

(4) Abel, R.; Young, T.; Farid, R.; Berne, B. J.; Friesner, R. A. Role of the Active-Site Solvent in the Thermodynamics of Factor Xa Ligand Binding. *J. Am. Chem. Soc.* **2008**, *130*, 2817−2831.

(5) Nguyen, C. N.; Kurtzman Young, T.; Gilson, M. K. Grid Inhomogeneous Solvation Theory: Hydration Structure and Thermodynamics of the Miniature Receptor Cucurbit[7]Uril. *J. Chem. Phys.* **2012**, *137*, 044101−044118.

(6) Deng, Y.; Roux, B. Computation of Binding Free Energy with Molecular Dynamics and Grand Canonical Monte Carlo Simulations. *J. Chem. Phys.* **2008**, *128*, 115103−115111.

(7) Michel, J.; Essex, J. W. Prediction of Protein-Ligand Binding Affinity by Free Energy Simulations: Assumptions, Pitfalls and Expectations. *J. Comput.-Aided Mol. Des.* **2010**, *24*, 639−658.

(8) Luccarelli, J.; Michel, J.; Tirado-Rives, J.; Jorgensen, W. L. Effects of Water Placement on Predictions of Binding Affinities for p38α MAP Kinase Inhibitors. *J. Chem. Theory Comput.* **2010**, *6*, 3850−3856.

(9) Mobley, D. L. Let's Get Honest About Sampling. *J. Comput.-Aided Mol. Des.* **2012**, *26*, 93−95.

(10) Beglov, D.; Roux, B. An Integral Equation to Describe the Solvation of Polar Molecules in Liquid Water. *J. Phys. Chem. B* **1997**, *101*, 7821−7826.

(11) Kovalenko, A.; Hirata, F. Three-Dimensional Density Profiles of Water in Contact with a Solute of Arbitrary Shape: a RISM Approach. *Chem. Phys. Lett.* **1998**, *290*, 237−244.

(12) Imai, T.; Hiraoka, R.; Kovalenko, A.; Hirata, F. Water Molecules in a Protein Cavity Detected by a Statistical−Mechanical Theory. *J. Am. Chem. Soc.* **2005**, *127*, 15334−15335.

(13) Imai, T.; Hiraoka, R.; Kovalenko, A.; Hirata, F. Locating Missing Water Molecules in Protein Cavities by the Three-Dimensional Reference Interaction Site Model Theory of Molecular Solvation. *Proteins* **2006**, *66*, 804−813.

(14) Yokogawa, D.; Sato, H.; Sakaki, S. The Position of Water Molecules in Bacteriorhodopsin: a Three-Dimensional Distribution Function Study. *Biophys. J.* **2009**, *147*, 112−116.

(15) Sindhikara, D. J.; Yoshida, N.; Hirata, F. Placevent: an Algorithm for Prediction of Explicit Solvent Atom Distribution-Application to HIV-1 Protease and F-ATP Synthase. *J. Comput. Chem.* **2012**, *33*, 1536−1543.

(16) Stumpe, M. C.; Blinov, N.; Wishart, D.; Kovalenko, A.; Pande, V. S. Calculation of Local Water Densities in Biological Systems: a Comparison of Molecular Dynamics Simulations and the 3D-RISM-KH Molecular Theory of Solvation. *J. Phys. Chem. B* **2010**, *115*, 319−328.

(17) Watanabe, H. C.; Welke, K.; Sindhikara, D. J.; Hegemann, P.; Elstner, M. Towards an Understanding of Channelrhodopsin Function: Simulations Lead to Novel Insights of the Channel Mechanism. *J. Mol. Biol.* **2013**, *425*, 1795−1814.

(18) Phongphanphanee, S.; Yoshida, N.; Hirata, F. The Potential of Mean Force of Water and Ions in Aquaporin Channels Investigated by the 3D-RISM Method. *Biophys. J.* **2009**, *147*, 107−111.

(19) Yoshida, N.; Phongphanphanee, S.; Maruyama, Y.; Imai, T.; Hirata, F. Selective Ion-Binding by Protein Probed with the 3D-RISM Theory. *J. Am. Chem. Soc.* **2006**, *128*, 12042−12043.

(20) Sindhikara, D. J.; Yoshida, N.; Kataoka, M.; Hirata, F. Solvent Penetration in Photoactive Yellow Protein R52Q Mutant: a Theoretical Study. *J. Mol. Liq.* **2011**, *164*, 120−122.

(21) Palmer, D. S.; Frolov, A. I.; Ratkova, E. L.; Fedorov, M. V. Towards a Universal Method for Calculating Hydration Free Energies: a 3D Reference Interaction Site Model with Partial Molar Volume Correction. *J. Phys.: Condens. Matter* **2010**, *22*, 492101.

(22) Imai, T.; Oda, K.; Kovalenko, A.; Hirata, F.; Kidera, A. Ligand Mapping on Protein Surfaces by the 3D-RISM Theory: Toward Computational Fragment-Based Drug Design. *J. Am. Chem. Soc.* **2009**, *131*, 12430−12440.

(23) Imai, T.; Miyashita, N.; Sugita, Y.; Kovalenko, A.; Hirata, F.; Kidera, A. Functionality Mapping on Internal Surfaces of Multidrug Transporter AcrB Based on Molecular Theory of Solvation: Implications for Drug Efflux Pathway. *J. Phys. Chem. B* **2011**, *115*, 8288−8295.

(24) Nikolic, D.; Blinov, N.; Wishart, D. S.; Kovalenko, A. 3D-RISM-Dock: a New Fragment-Based Drug Design Protocol. *J. Chem. Theory Comput.* **2012**.

(25) Kiyota, Y.; Yoshida, N.; Hirata, F. A New Approach for Investigating the Molecular Recognition of Protein: Toward Structure-Based Drug Design Based on the 3D-RISM Theory. *J. Chem. Theory Comput.* **2011**, *7*, 3803−3815.

(26) Gusarov, S.; Pujari, B. S.; Kovalenko, A. Efficient Treatment of Solvation Shells in 3D Molecular Theory of Solvation. *J. Comput. Chem.* **2012**, *33*, 1478−1494.

(27) Maruyama, Y.; Hirata, F. Modified Anderson Method for Accelerating 3D-RISM Calculations Using Graphics Processing Unit. *J. Chem. Theory Comput.* **2012**, *8*, 3015−3021.

(28) Hirano, K.; Yokogawa, D.; Sato, H.; Sakaki, S. An Analysis of 3D Solvation Structure in Biomolecules: Application to Coiled Coil Serine and Bacteriorhodopsin. *J. Phys. Chem. B* **2010**, *114*, 7935−7941.

(29) Wodak, S. J.; Janin, J. Computer Analysis of Protein-Protein Interaction. *J. Mol. Biol.* **1978**, *124*, 323−342.

(30) Mitchell, J. C. Sampling Rotation Groups by Successive Orthogonal Images. *SIAM J. Sci. Comput.* **2008**, *30*, 525−547.

(31) Yershova, A.; Jain, S.; LaValle, S. M.; Mitchell, J. C. Generating Uniform Incremental Grids on SO(3) Using the Hopf Fibration. *Int. J. Robot. Res.* **2010**, *29*, 801−812.

(32) Hirata, F. In *Molecular Theory of Solvation*; Fumio, H., Ed.; Kluwer Academic Publishers: Dordrecht, 2003.

(33) Imai, T.; Kovalenko, A.; Hirata, F. Partial Molar Volume of Proteins Studied by the Three-Dimensional Reference Interaction Site Model Theory. *J. Phys. Chem. B* **2005**, *109*, 6658−6665.

(34) Lazaridis, T.; Karplus, M. Orientational Correlations and Entropy in Liquid Water. *J. Chem. Phys.* **1996**, *105*, 4294−4316.

(35) Case, D. A.; Darden, T. A.; Cheatham, T. E., III; Simmerling, C. L.; Wang, J.; Duke, R. E.; Luo, R.; Walker, R. C.; Zhang, W.; Merz, K. M.; et al. *AMBER 12*; University of California: CA, 2012.

(36) Adachi, M.; Ohhara, T.; Kurihara, K.; Tamada, T.; Honjo, E.; Okazaki, N.; Arai, S.; Shoyama, Y.; Kimura, K.; Matsumura, H. Structure of HIV-1 Protease in Complex with Potent Inhibitor KNI-272 Determined by High-Resolution X-Ray and Neutron Crystallography. *Proc. Natl. Acad. Sci. U.S.A.* **2009**, *106*, 4641−4646.

(37) Hornak, V.; Abel, R.; Okur, A.; Strockbine, B.; Roitberg, A.; Simmerling, C. Comparison of Multiple Amber Force Fields and Development of Improved Protein Backbone Parameters. *J. Comput. Chem.* **2006**, *65*, 712−725.

(38) Frisch, M. J.; Trucks, G. W.; Schlegel, H. B.; Scuseria, G. E.; Robb, M. A.; Cheeseman, J. R.; Scalmani, G.; Barone, V.; Mennucci, B.; Petersson, G. A.; et al. *Gaussian 09*; Gaussian, Inc.: Wallingford, CT, 2009; Vol. 2, p 4.
(39) Wang, J.; Wolf, R. M.; Caldwell, J. W.; Kollman, P. A.; Case, D. A. Development and Testing of a General Amber Force Field. *J. Comput. Chem.* **2004**, *25*, 1157−1174.
(40) Word, J. M.; Lovell, S. C.; Richardson, J. S.; Richardson, D. C. Asparagine and Glutamine: Using Hydrogen Atom Contacts in the Choice of Side-Chain Amide Orientation. *J. Mol. Biol.* **1999**, *285*, 1735−1747.
(41) Dupradeau, F.-Y.; Pigache, A.; Zaffran, T.; Savineau, C.; Lelong, R.; Grivel, N.; Lelong, D.; Rosanski, W.; Cieplak, P. The R.E.D. Tools: Advances in RESP and ESP Charge Derivation and Force Field Library Building. *Phys. Chem. Chem. Phys.* **2010**, *12*, 7821.
(42) Luchko, T.; Gusarov, S.; Roe, D. R.; Simmerling, C.; Case, D. A.; Tuszynski, J.; Kovalenko, A. Three-Dimensional Molecular Theory of Solvation Coupled with Molecular Dynamics in Amber. *J. Chem. Theory Comput.* **2010**, *6*, 607−624.
(43) Li, Z.; Lazaridis, T. Thermodynamic Contributions of the Ordered Water Molecule in HIV-1 Protease. *J. Am. Chem. Soc.* **2003**, *125*, 6636−6637.
(44) Baldwin, E. T.; Bhat, T. N.; Gulnik, S.; Liu, B.; Topol, I. A.; Kiso, Y.; Mimoto, T.; Mitsuya, H.; Erickson, J. W. Structure of HIV-1 Protease with KNI-272, a Tight-Binding Transition-State Analog Containing Allophenylnorstatine. *Biophys. J.* **1995**, *3*, 581−590.